Science
AAAS

Supplementary Materials for

Spatial transcriptomics of planktonic and sessile bacterial populations at single-cell resolution

Daniel Dar *et al.*

Corresponding authors: Dianne K. Newman, dkn@caltech.edu; Long Cai, lcai@caltech.edu

Science **373**, eabi4882 (2021)
DOI: 10.1126/science.abi4882

The PDF file includes:

Figs. S1 to S8
Tables S1, S3, and S4
Caption for Table S2

Other Supplementary Material for this manuscript includes the following:

MDAR Reproducibility Checklist (PDF)
Table S2 (Excel)

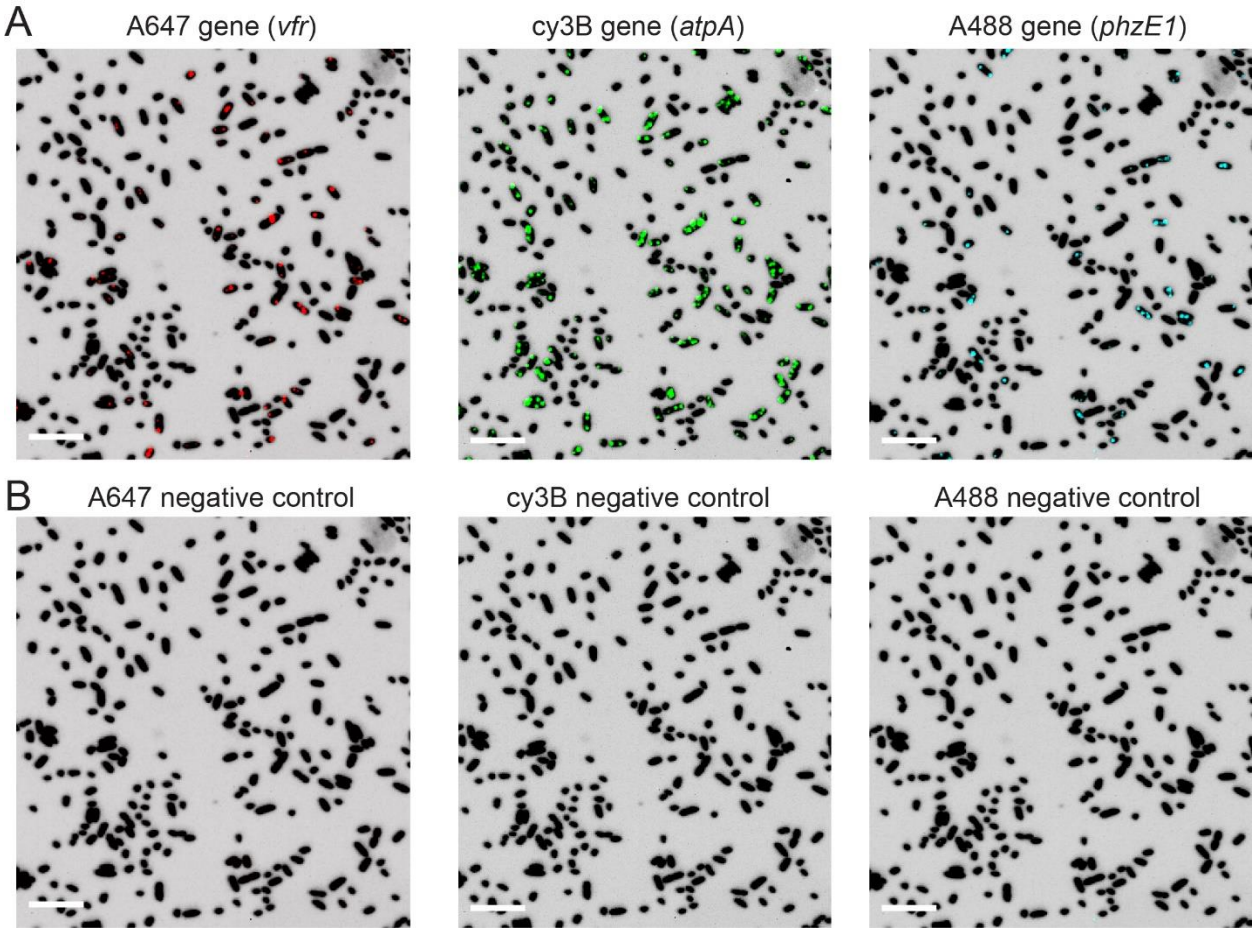

Fig. S1.

Negative control genes estimate the false positive rate. (A) Examples of positive signal for genes labeled with one of the three fluorophores used in this study A647 (red), cy3B (green), and A488 (cyan). For context, the mRNA-FISH fluorescence is shown over DAPI (dark silhouette). (B) Same regions as in panel A, but showing the raw fluorescence of the negative control genes for each fluorophore. For direct comparison, the intensity range is identical between positive and negative panels in A-B. Scale bar represents 5µm.

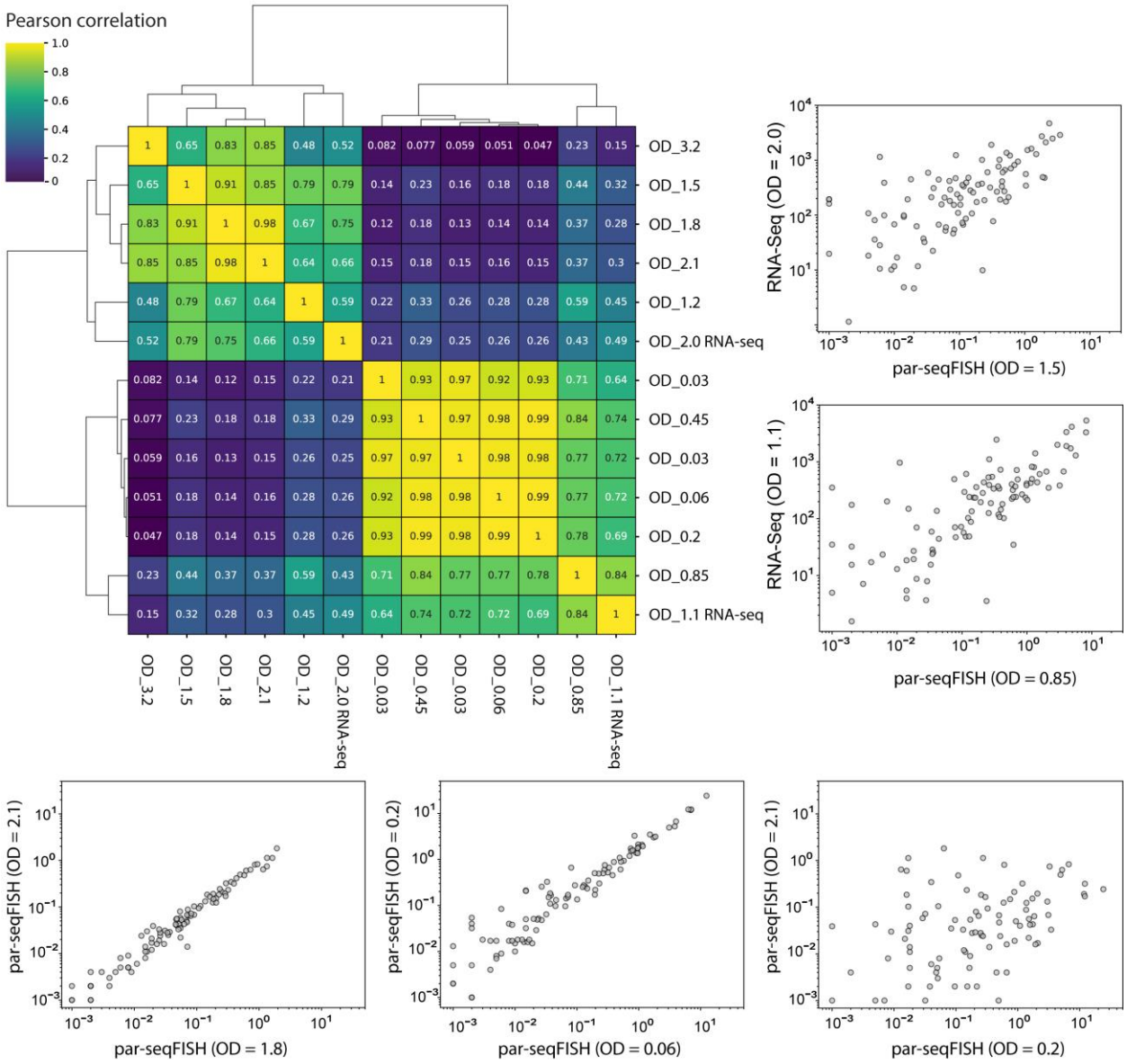

Fig. S2.

Correlation analysis between seqFISH and RNA-Seq. A clustered correlation matrix was calculated using the average par-seqFISH expression measurement for each time-point in the LB growth curve and the normalized RNA-Seq expression, reads per kilobase per million (RPKM), from a previously published study performed under similar conditions (*51*). The conditions are noted to the side along with their respective OD_{600} values (e.g., LB_0.2 represent cells collected when the OD_{600} of the LB culture reached 0.2). The Pearson correlation is shown as a color map and indicated in the figure. Scatter plots showing RNA-seq and par-seqFISH comparisons are displayed on the right. RNA-seq axis shows the RPKM and the par-seqFISH axis shows the average mRNA number per cell. Scatters comparing different time points in the par-seqFISH experiment are shown below. The X and Y axes show the average mRNA number per cell.

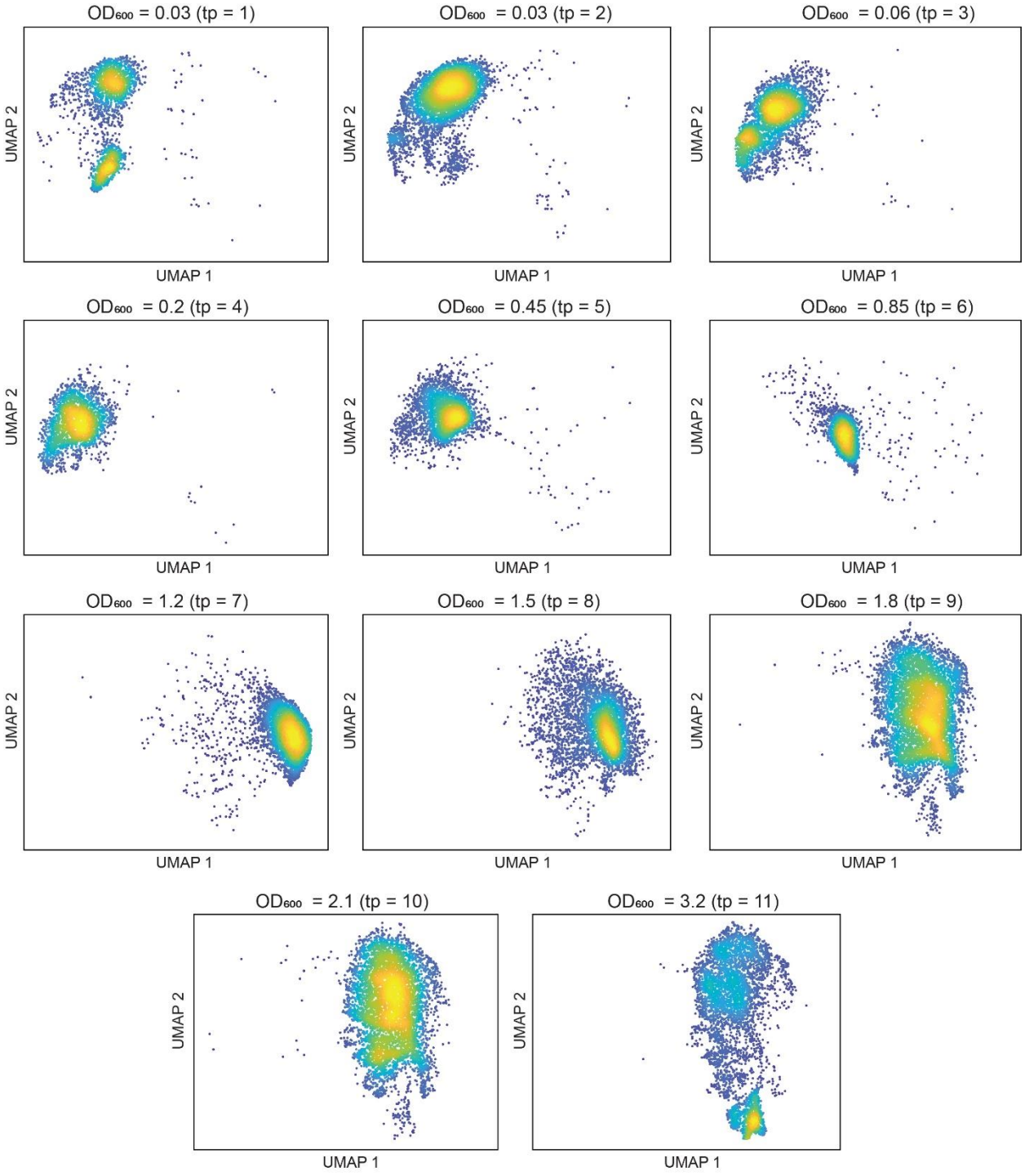

Fig. S3.

Single-cell dispersions in UMAP space for each growth curve time point. A UMAP density plot of cells belonging to specific time points. The OD_{600} values and the number of the time points are shown over each plot. Color intensity represents cell density.

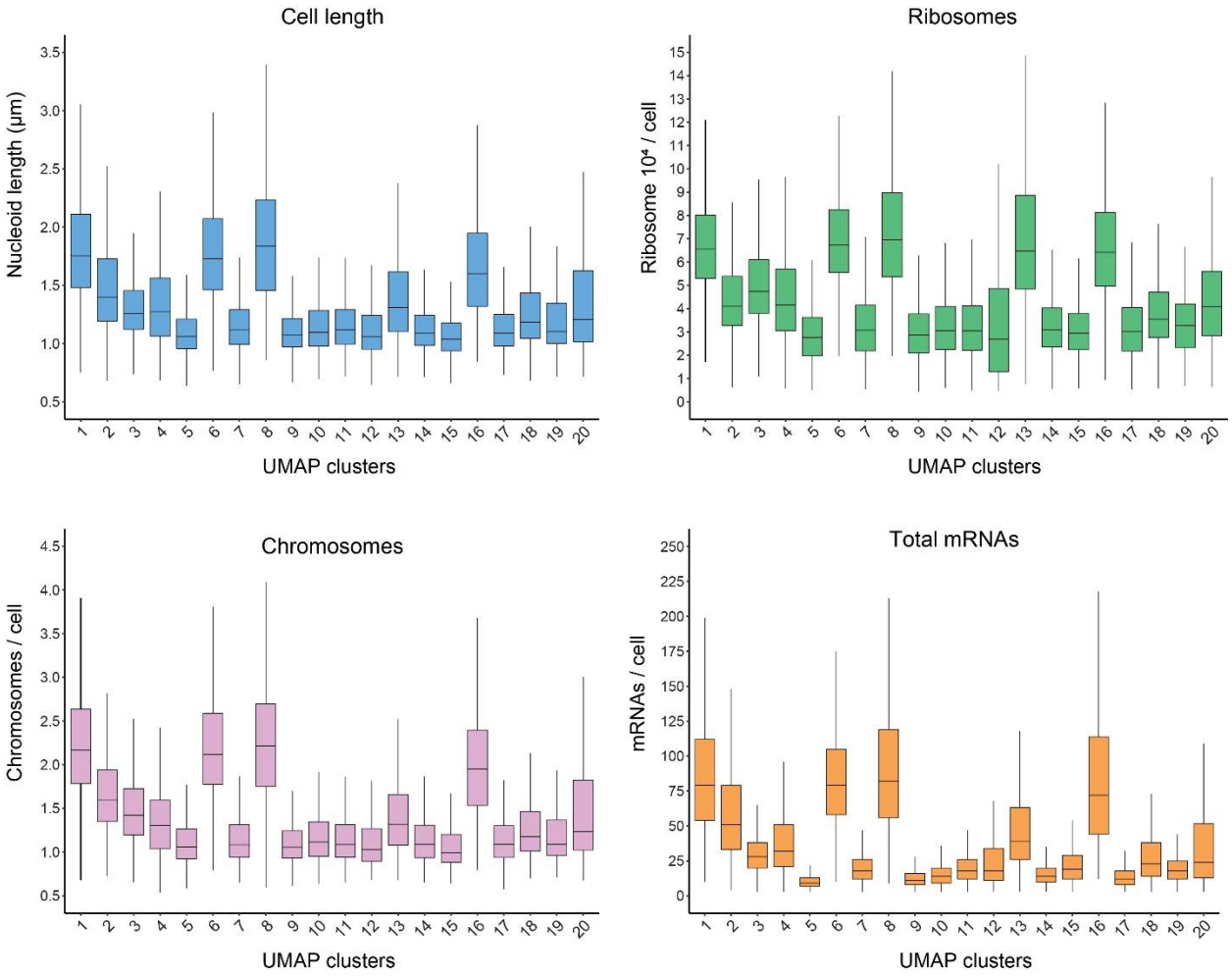

Fig. S4.

Distributions of single-cell parameters across the detected UMAP clusters. Distributions of nucleoid length, chromosome copy, ribosome levels and total mRNAs for each of the UMAP clusters described in main Fig. 3.

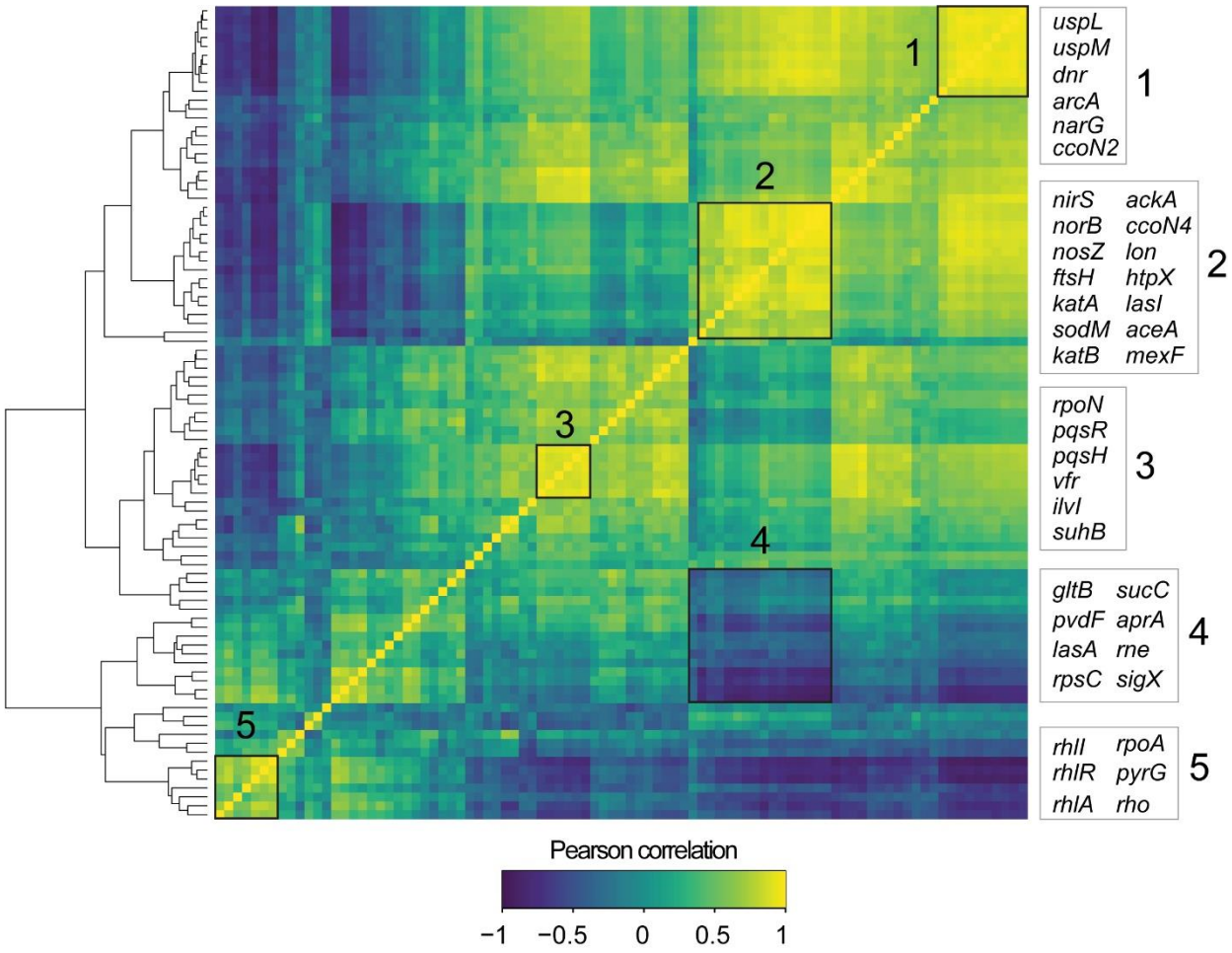

Fig. S5.

Spatial correlation analysis. Gene centered neighborhood analysis for detecting spatial correlation. For each gene, its 99th percentile expressing cells were identified and their 5 immediate neighbors within 3 µm were collected (leaving out the enriched center cell). The set of all such neighbors across the experiment was analyzed together to produce a mean expression profile that was compared with the total population to produce a local enrichment/depletion ratio. The Pearson correlation between such gene neighborhood profiles was calculated and is shown as a clustered heat map. Five selected regions are highlighted and numbered. Key genes within each cluster are described to the right.

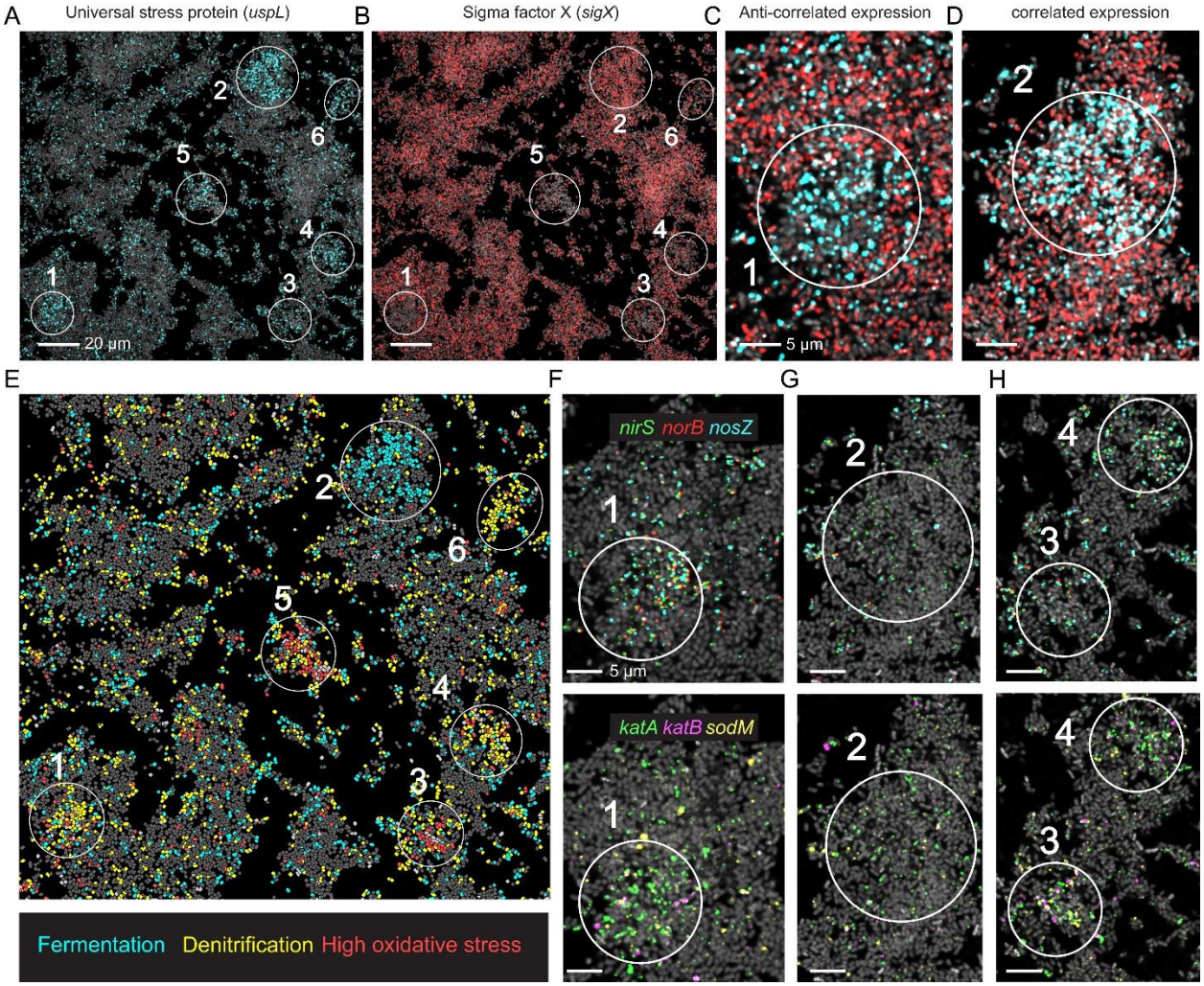

Fig. S6.

Distributions of single-cell parameters per UMAP cluster. (**A**-**B**) Representative 10h microaggregates. Cells are shown via 16S rRNA FISH fluorescence (gray) and overlayed with gene-expression as indicated in each panel. White circles highlight regions of interest. (**C**-**D**) Zoom-in on region 1 and 2 showing *uspL* (cyan) and *sigX* (red). (**E**) Cells painted according to their neighborhood class as indicated in the panel legend. (**F**-**H**) Zoom-in highlighted regions overlaid with raw gene-expression as indicated in the panel legends.

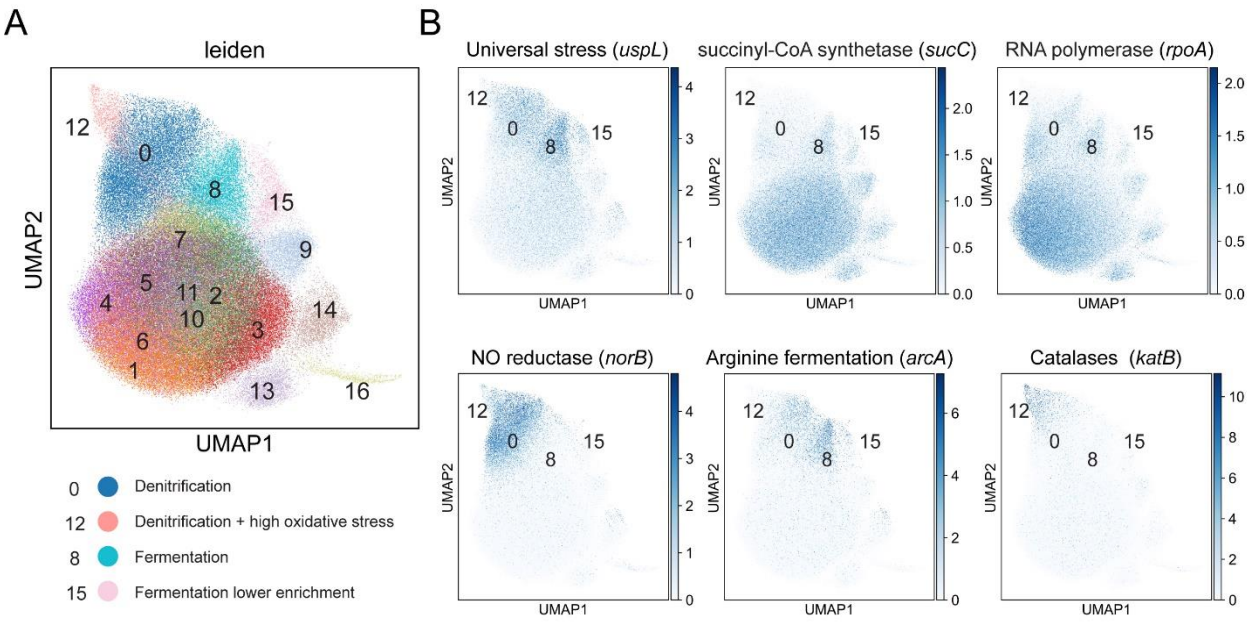

Fig. S7.

UMAP analysis of 10h biofilms. (**A**) UMAP analysis was performed using the 10h biofilm experiment. Below, clusters are labeled and are divided into predicted metabolic groups. (**B**) UMAP overlaid with specific gene data. The color map shows the normalized expression scaled to unit variance. The cluster number positions are shown in the figure.

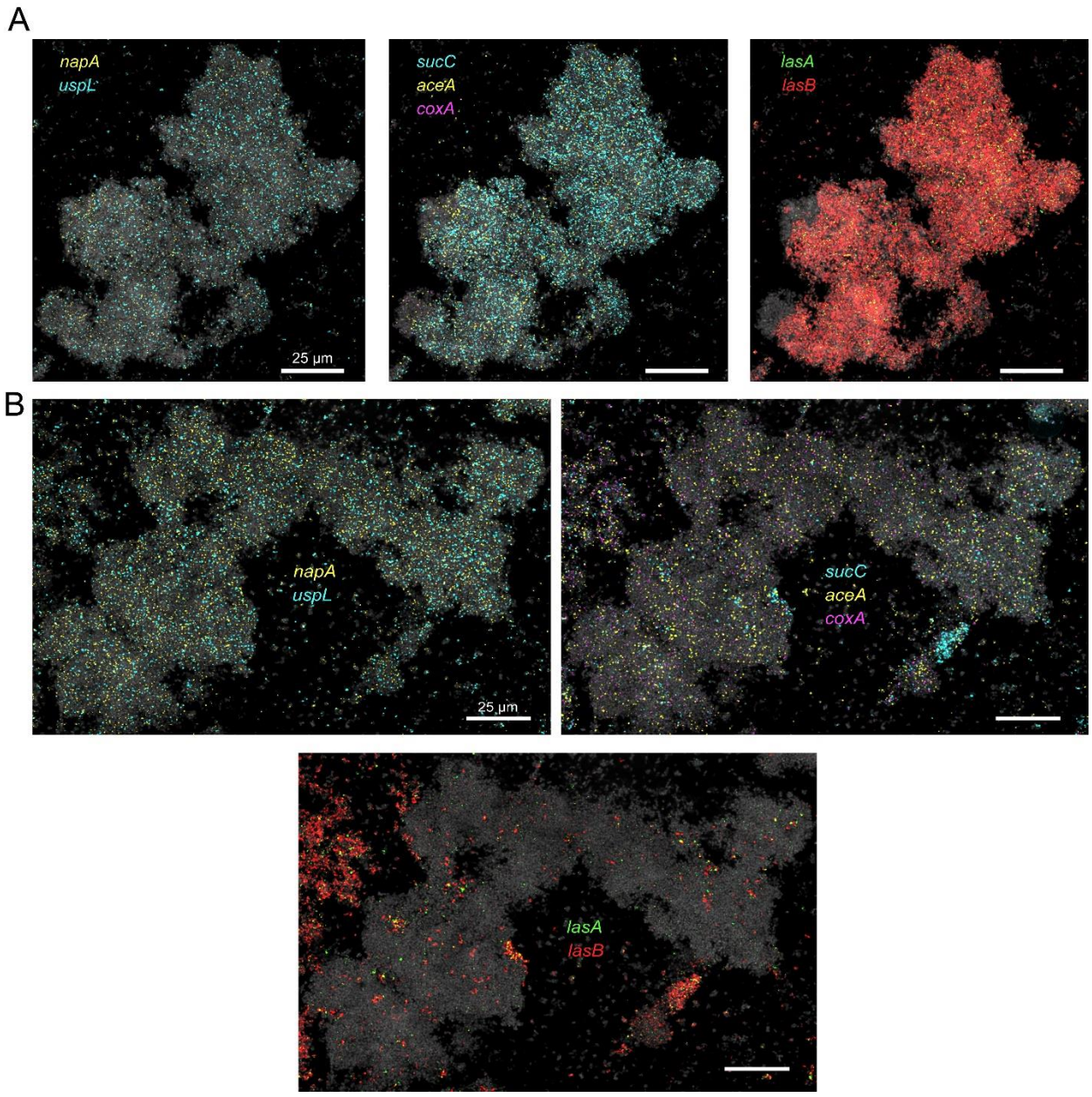

Fig. S8.

Functional zonation in 35h microaggregates. (**A**-**B**) Various *P. aeruginosa* 35h aggregates. Bacteria are shown via 16S rRNA FISH fluorescence (gray) and are overlaid with raw mRNA-FISH fluorescence for several genes as described in the images.

Table S1.
Gene library used in study.

Locus_tag	Gene name	Gene description
P1_gp003	*cre*	Phage P1 negative control gene
P1_gp013	*pro*	Phage P1 negative control gene
P1_gp078	*dbn*	Phage P1 negative control gene
PA14_00010	*dnaA*	chromosomal replication initiator protein DnaA
PA14_00560	*exoT*	exoenzyme T
PA14_00640	*phzH*	phenazine-modifying enzyme
PA14_01160	*vgrG*	T6SS protein
PA14_01300	*coxA*	cytochrome c oxidase, subunit I
PA14_01720	*ahpF*	alkyl hydroperoxide reductase subunit F
PA14_01970	*TriC*	Triclosan RND efflux transporter
PA14_03650	*cysA*	sulfate transport protein CysA
PA14_03920	*spuD*	polyamine transport protein
PA14_04410	*ptsP*	phosphoenolpyruvate-protein phosphotransferase
PA14_04930	*rpoH*	RNA polymerase sigma-32 factor
PA14_05310	*gshB*	glutathione synthetase
PA14_05540	*mexB*	RND multidrug efflux transporter MexB
PA14_06750	*nirS*	nitrite reductase precursor
PA14_06830	*norB*	nitric-oxide reductase subunit B
PA14_06870	*dnr*	transcriptional regulator Dnr
PA14_07520	*rpoD*	sigma factor RpoD
PA14_08150	*PA14_08150*	Pyocin R2 F2 operon
PA14_08370	*vfr*	cyclic AMP receptor-like protein
PA14_08910	*rpsC*	30S ribosomal protein S3
PA14_09115	*rpoA*	DNA-directed RNA polymerase alpha chain
PA14_09150	*katA*	catalase
PA14_09280	*pchF*	pyochelin synthetase PchF
PA14_09400	*phzS*	flavin-containing monooxygenase
PA14_09440	*phzE1*	phenazine biosynthesis protein PhzE
PA14_09490	*phzM*	phenazine-specific methyltransferase
PA14_09520	*mexI*	probable RND efflux transporter
PA14_10500	*ccoN4*	cytochrome c oxidase subunit (cbb3-type)
PA14_10790	*ampC*	cephalosporinase
PA14_13780	*narG*	respiratory nitrate reductase alpha subun
PA14_14680	*suhB*	extragenic suppressor protein SuhB
PA14_16250	*lasB*	elastase LasB
PA14_16500	*wspR*	two-component response regulator
PA14_17290	*pyrG*	CTP synthase
PA14_17480	*rpoS*	sigma factor RpoS

PA14_17530	*recA*	RecA protein
PA14_18580	*algD*	GDP-mannose 6-dehydrogenase AlgD
PA14_19100	*rhlA*	rhamnosyltransferase chain A
PA14_19120	*rhlR*	acylhomoserine lactone dependent transcriptional regulator
PA14_19130	*rhlI*	autoinducer synthesis protein RhlI
PA14_20200	*nosZ*	nitrous-oxide reductase precursor
PA14_22980	*gltB*	binding protein component of ABC sugar transporter
PA14_23920	*purF*	amidophosphoribosyltransferase
PA14_24480	*pelA*	conserved hypothetical protein
PA14_25080	*fadB*	fatty-acid oxidation complex alpha-subunit
PA14_25560	*rne*	ribonuclease E
PA14_27480	*htpX*	heat shock protein HtpX
PA14_30050	*aceA*	isocitrate lyase
PA14_30630	*pqsH*	FAD-dependent monooxygenase
PA14_32390	*mexF*	RND multidrug efflux transporter MexF
PA14_33700	*pvdF*	pyoverdine synthetase F
PA14_34050	*impC*	conserved hypothetical protein
PA14_35670	*pslG*	glycosyl hydrolase
PA14_36310	*hcnC*	hydrogen cyanide synthase HcnC
PA14_36345	*exoY*	adenylate cyclase ExoY
PA14_38410	*amrB*	RND multidrug efflux transporter
PA14_39330	*rbsA*	ribose ABC transporter, ATP-binding protein
PA14_40290	*lasA*	staphylolytic protease preproenzyme LasA
PA14_40510	*ccoN3*	cytochrome c oxidase, cbb3-type, subunit
PA14_41220	*lon*	Lon protease
PA14_41230	*clpX*	ATP-dependent Clp protease ATP-binding subunit ClpX
PA14_41440	*uspL*	universal stress protein
PA14_41510	*nasA*	nitrate transporter
PA14_41575	*sigX*	ECF sigma factor SigX
PA14_42350	*pscC*	Type III secretion outer membrane protein PscC precursor
PA14_42500	*pcrD*	type III secretory apparatus protein PcrD
PA14_43950	*sucC*	succinyl-CoA synthetase beta subunit
PA14_44340	*ccoN2*	cytochrome oxidase subunit (cbb3-type)
PA14_44370	*ccoN1*	cytochrome oxidase subunit (cbb3-type)
PA14_44490	*anr*	transcriptional regulator Anr
PA14_45630	*fliA*	motility sigma factor FliA
PA14_45940	*lasI*	autoinducer synthesis protein LasI
PA14_45960	*lasR*	transcriptional regulator LasR
PA14_48060	*aprA*	alkaline metalloproteinase precursor
PA14_48930	*PA14_48930*	pf5 phage gene
PA14_49250	*napA*	periplasmic nitrate reductase protein NapA

PA14_50290	*fliC*	flagellin type B
PA14_50360	*flgK*	flagellar hook-associated protein 1 FlgK
PA14_51340	*mvfR*	Transcriptional regulator MvfR
PA14_51410	*pqsC*	PqsC
PA14_52180	*relA*	GTP pyrophosphokinase
PA14_52270	*ldhA*	D-lactate dehydrogenase (fermentative)
PA14_52580	*lysC*	aspartate kinase alpha and beta chain
PA14_53470	*ackA*	probable acetate kinase
PA14_54430	*algU*	sigma factor AlgU
PA14_56220	*uspM*	universal stress protein
PA14_56780	*sodB*	iron superoxide dismutase
PA14_57940	*rpoN*	RNA polymerase sigma-54 factor
PA14_58000	*sodM*	superoxide dismutase
PA14_58730	*pilA*	type IV pilin structural subunit
PA14_60310	*pilY1*	type 4 fimbrial biogenesis protein PilY1
PA14_61040	*katB*	catalase
PA14_61060	*fnr-2*	ferredoxin--NADP+ reductase
PA14_61200	*cdrA*	conserved hypothetical protein
PA14_62160	*ilvI*	acetolactate synthase large subunit
PA14_62710	*pnp*	polyribonucleotide nucleotidyltransferase
PA14_62730	*truB*	tRNA pseudouridine 55 synthase
PA14_62860	*ftsH*	cell division protein FtsH
PA14_68330	*arcA*	Arginine fermentation
PA14_69190	*rho*	transcription termination factor Rho
PA14_70470	*spoT*	guanosine-3',5'-bis(diphosphate) 3'-pyrophosphohydrolase
PA14_70560	*OxyR*	transcriptional regulator, LysR family
PA14_70860	*pstS*	phosphate ABC transporter, periplasmic phosphate-binding protein
PA14_72960	*kgtP*	MFS dicarboxylate transporter
PA14_73260	*atpA*	ATP synthase alpha chain

Table S3.
16S rRNA probes used in study.

Probe_id	16S pos	Probe sequence
Ribo-Tag_1	771-799	CGATTAGTCGTCACTAAGCGTGGACTACCAGGGTATCTAATCCTGAAACTCCGAATGCTACG
Ribo-Tag_2	771-799	CGATTAGTCGTCACTAAGCGTGGACTACCAGGGTATCTAATCCTGAAGGTTACACGCGACTA
Ribo-Tag_3	771-799	ACTCCGAATGCTACGAAGCGTGGACTACCAGGGTATCTAATCCTGAAGGTTACACGCGACTA
Ribo-Tag_4	771-799	ATGTAACCAAGCGTCAAGCGTGGACTACCAGGGTATCTAATCCTGAATCAGTTACCGGTGTA
Ribo-Tag_5	771-799	ATGTAACCAAGCGTCAAGCGTGGACTACCAGGGTATCTAATCCTGAATCCAGCTTACGTTCG
Ribo-Tag_6	771-799	TCAGTTACCGGTGTAAAGCGTGGACTACCAGGGTATCTAATCCTGAATCCAGCTTACGTTCG
Ribo-Tag_7	771-799	CGATTAGTCGTCACTAAGCGTGGACTACCAGGGTATCTAATCCTGAATCAGTTACCGGTGTA
Ribo-Tag_8	771-799	CGATTAGTCGTCACTAAGCGTGGACTACCAGGGTATCTAATCCTGAATCCAGCTTACGTTCG
Ribo-Tag_9	771-799	ATGTAACCAAGCGTCAAGCGTGGACTACCAGGGTATCTAATCCTGAAACTCCGAATGCTACG
Ribo-Tag_10	771-799	ATGTAACCAAGCGTCAAGCGTGGACTACCAGGGTATCTAATCCTGAAGGTTACACGCGACTA
Ribo-Tag_11	771-799	ACTCCGAATGCTACGAAGCGTGGACTACCAGGGTATCTAATCCTGAATCCAGCTTACGTTCG
Ribo-Tag_12	771-799	TCAGTTACCGGTGTAAAGCGTGGACTACCAGGGTATCTAATCCTGAAGGTTACACGCGACTA
Reference (all)	714-743	TATGTGACTACGCACAACGTCGTATCCAGTATAACAGTGTCAGTATCAGTCCAGGTGGTCGCCTAACTATTATCGCCGAGA

Table S4.
UMAP cluster frequency (%) per LB growth condition.

Cluster	OD 0.03 (lag_0.5h)	OD 0.03 (lag_1h)	OD 0.06	OD_0.2	OD_0.45	OD_0.85	OD_1.2	OD_1.5	OD_1.8	OD_2.1	OD_3.2
1	6.71%	29.94%	45.89%	56.18%	74.52%	2.31%	0.05%	0.00%	0.02%	0.00%	0.00%
2	0.04%	0.02%	0.00%	0.09%	0.03%	0.27%	88.59%	17.43%	0.82%	0.87%	0.75%
3	53.44%	47.55%	12.96%	3.52%	6.33%	1.93%	0.02%	0.02%	0.21%	0.19%	0.04%
4	0.00%	0.00%	0.00%	0.00%	0.07%	0.15%	2.38%	31.72%	19.97%	15.96%	7.10%
5	0.22%	0.13%	0.03%	0.00%	0.00%	0.08%	0.86%	8.23%	17.19%	20.77%	21.23%
6	0.04%	0.02%	0.09%	0.05%	2.80%	92.22%	0.66%	0.44%	0.15%	0.05%	0.04%
7	0.13%	0.04%	0.00%	0.00%	0.17%	0.50%	1.45%	9.83%	12.33%	13.91%	9.46%
8	0.61%	8.05%	30.30%	28.34%	9.33%	0.31%	0.00%	0.02%	0.02%	0.03%	0.00%
9	0.17%	0.11%	0.03%	0.00%	0.00%	0.12%	0.52%	4.76%	9.74%	9.32%	9.94%
10	0.04%	0.16%	0.03%	0.05%	0.17%	0.27%	0.70%	4.78%	8.37%	10.13%	7.47%
11	0.35%	0.40%	0.18%	0.27%	0.31%	0.69%	1.31%	4.49%	7.71%	8.61%	7.08%
12	0.09%	0.09%	0.00%	0.14%	0.35%	0.08%	0.38%	0.46%	1.35%	1.50%	23.30%
13	34.56%	5.03%	1.80%	1.85%	1.73%	0.12%	0.18%	0.53%	0.71%	0.65%	0.42%
14	0.04%	0.04%	0.03%	0.00%	0.03%	0.23%	0.88%	5.10%	6.82%	6.53%	3.78%
15	0.13%	0.04%	0.00%	0.00%	0.03%	0.27%	1.04%	5.80%	6.55%	4.67%	3.82%
16	2.90%	8.09%	8.19%	8.94%	2.73%	0.12%	0.00%	0.00%	0.00%	0.02%	0.00%
17	0.17%	0.04%	0.12%	0.00%	0.07%	0.04%	0.23%	2.04%	3.16%	2.73%	3.76%
18	0.04%	0.02%	0.03%	0.00%	0.07%	0.08%	0.29%	2.77%	2.74%	2.15%	0.39%
19	0.09%	0.02%	0.00%	0.00%	0.00%	0.12%	0.29%	0.73%	1.42%	1.47%	0.62%
20	0.22%	0.18%	0.31%	0.59%	1.24%	0.12%	0.16%	0.85%	0.74%	0.44%	0.81%

Caption for Table S2: Gene library used in this study.

References and Notes

1. H.-C. Flemming, S. Wuertz, Bacteria and archaea on Earth and their abundance in biofilms. *Nat. Rev. Microbiol.* **17**, 247–260 (2019). doi:10.1038/s41579-019-0158-9 Medline

2. J. W. Costerton, K. J. Cheng, G. G. Geesey, T. I. Ladd, J. C. Nickel, M. Dasgupta, T. J. Marrie, Bacterial biofilms in nature and disease. *Annu. Rev. Microbiol.* **41**, 435–464 (1987). doi:10.1146/annurev.mi.41.100187.002251 Medline

3. W. H. DePas, R. Starwalt-Lee, L. Van Sambeek, S. Ravindra Kumar, V. Gradinaru, D. K. Newman, Exposing the three-dimensional biogeography and metabolic states of pathogens in cystic fibrosis sputum via hydrogel embedding, clearing, and rRNA labeling. *mBio* **7**, e00796 (2016). doi:10.1128/mBio.00796-16 Medline

4. J. L. Mark Welch, B. J. Rossetti, C. W. Rieken, F. E. Dewhirst, G. G. Borisy, Biogeography of a human oral microbiome at the micron scale. *Proc. Natl. Acad. Sci. U.S.A.* **113**, E791–E800 (2016). doi:10.1073/pnas.1522149113 Medline

5. J. A. Schaber, W. J. Triffo, S. J. Suh, J. W. Oliver, M. C. Hastert, J. A. Griswold, M. Auer, A. N. Hamood, K. P. Rumbaugh, *Pseudomonas aeruginosa* forms biofilms in acute infection independent of cell-to-cell signaling. *Infect. Immun.* **75**, 3715–3721 (2007). doi:10.1128/IAI.00586-07 Medline

6. P. Jorth, M. A. Spero, J. Livingston, D. K. Newman, Quantitative visualization of gene expression in mucoid and nonmucoid *Pseudomonas aeruginosa* aggregates reveals localized peak expression of alginate in the hypoxic zone. *mBio* **10**, e02622 (2019). doi:10.1128/mBio.02622-19 Medline

7. R. Hatzenpichler, V. Krukenberg, R. L. Spietz, Z. J. Jay, Next-generation physiology approaches to study microbiome function at single cell level. *Nat. Rev. Microbiol.* **18**, 241–256 (2020). doi:10.1038/s41579-020-0323-1 Medline

8. G. L. Chadwick, F. Jiménez Otero, J. A. Gralnick, D. R. Bond, V. J. Orphan, NanoSIMS imaging reveals metabolic stratification within current-producing biofilms. *Proc. Natl. Acad. Sci. U.S.A.* **116**, 20716–20724 (2019). doi:10.1073/pnas.1912498116 Medline

9. M. Ackermann, A functional perspective on phenotypic heterogeneity in microorganisms. *Nat. Rev. Microbiol.* **13**, 497–508 (2015). doi:10.1038/nrmicro3491 Medline

10. C. R. Evans, C. P. Kempes, A. Price-Whelan, L. E. P. Dietrich, Metabolic heterogeneity and cross-feeding in bacterial multicellular systems. *Trends Microbiol.* **28**, 732–743 (2020). doi:10.1016/j.tim.2020.03.008 Medline

11. F. Schreiber, S. Littmann, G. Lavik, S. Escrig, A. Meibom, M. M. M. Kuypers, M. Ackermann, Phenotypic heterogeneity driven by nutrient limitation promotes growth in fluctuating environments. *Nat. Microbiol.* **1**, 16055 (2016). doi:10.1038/nmicrobiol.2016.55 Medline

12. F. Schreiber, M. Ackermann, Environmental drivers of metabolic heterogeneity in clonal microbial populations. *Curr. Opin. Biotechnol.* **62**, 202–211 (2020). doi:10.1016/j.copbio.2019.11.018 Medline

13. S. H. Kopf, S. E. McGlynn, A. Green-Saxena, Y. Guan, D. K. Newman, V. J. Orphan, Heavy water and (15) N labelling with NanoSIMS analysis reveals growth rate-dependent metabolic heterogeneity in chemostats. *Environ. Microbiol.* **17**, 2542–2556 (2015). doi:10.1111/1462-2920.12752 Medline

14. J.-W. Veening, W. K. Smits, O. P. Kuipers, Bistability, epigenetics, and bet-hedging in bacteria. *Annu. Rev. Microbiol.* **62**, 193–210 (2008). doi:10.1146/annurev.micro.62.081307.163002 Medline

15. A. Z. Rosenthal, Y. Qi, S. Hormoz, J. Park, S. H.-J. Li, M. B. Elowitz, Metabolic interactions between dynamic bacterial subpopulations. *eLife* **7**, e33099 (2018). doi:10.7554/eLife.33099 Medline

16. C. R. Armbruster, C. K. Lee, J. Parker-Gilham, J. de Anda, A. Xia, K. Zhao, K. Murakami, B. S. Tseng, L. R. Hoffman, F. Jin, C. S. Harwood, G. C. Wong, M. R. Parsek, Heterogeneity in surface sensing suggests a division of labor in *Pseudomonas aeruginosa* populations. *eLife* **8**, e45084 (2019). doi:10.7554/eLife.45084 Medline

17. M. Diard, V. Garcia, L. Maier, M. N. P. Remus-Emsermann, R. R. Regoes, M. Ackermann, W.-D. Hardt, Stabilization of cooperative virulence by the expression of an avirulent phenotype. *Nature* **494**, 353–356 (2013). doi:10.1038/nature11913 Medline

18. P. S. Stewart, M. J. Franklin, Physiological heterogeneity in biofilms. *Nat. Rev. Microbiol.* **6**, 199–210 (2008). doi:10.1038/nrmicro1838 Medline

19. P. S. Stewart, Diffusion in biofilms. *J. Bacteriol.* **185**, 1485–1491 (2003). doi:10.1128/JB.185.5.1485-1491.2003 Medline

20. E. Wolfsberg, C. P. Long, M. R. Antoniewicz, Metabolism in dense microbial colonies: ^{13}C metabolic flux analysis of E. coli grown on agar identifies two distinct cell populations with acetate cross-feeding. *Metab. Eng.* **49**, 242–247 (2018). doi:10.1016/j.ymben.2018.08.013 Medline

21. O. Kotte, B. Volkmer, J. L. Radzikowski, M. Heinemann, Phenotypic bistability in *Escherichia coli*'s central carbon metabolism. *Mol. Syst. Biol.* **10**, 736 (2014). doi:10.15252/msb.20135022 Medline

22. F. Bocci, Y. Suzuki, M. Lu, J. N. Onuchic, Role of metabolic spatiotemporal dynamics in regulating biofilm colony expansion. *Proc. Natl. Acad. Sci. U.S.A.* **115**, 4288–4293 (2018). doi:10.1073/pnas.1706920115 Medline

23. C. D. Nadell, K. Drescher, K. R. Foster, Spatial structure, cooperation and competition in biofilms. *Nat. Rev. Microbiol.* **14**, 589–600 (2016). doi:10.1038/nrmicro.2016.84 Medline

24. O. X. Cordero, M. S. Datta, Microbial interactions and community assembly at microscales. *Curr. Opin. Microbiol.* **31**, 227–234 (2016). doi:10.1016/j.mib.2016.03.015 Medline

25. H. Shi, Q. Shi, B. Grodner, J. S. Lenz, W. R. Zipfel, I. L. Brito, I. De Vlaminck, Highly multiplexed spatial mapping of microbial communities. *Nature* **588**, 676–681 (2020). doi:10.1038/s41586-020-2983-4 Medline

26. C. Tropini, K. A. Earle, K. C. Huang, J. L. Sonnenburg, The gut microbiome: Connecting spatial organization to function. *Cell Host Microbe* **21**, 433–442 (2017). doi:10.1016/j.chom.2017.03.010 Medline

27. S. A. Wilbert, J. L. Mark Welch, G. G. Borisy, Spatial ecology of the human tongue dorsum microbiome. *Cell Rep.* **30**, 4003–4015.e3 (2020). doi:10.1016/j.celrep.2020.02.097 Medline

28. F. Imdahl, E. Vafadarnejad, C. Homberger, A.-E. Saliba, J. Vogel, Single-cell RNA-sequencing reports growth-condition-specific global transcriptomes of individual bacteria. *Nat. Microbiol.* **5**, 1202–1206 (2020). doi:10.1038/s41564-020-0774-1 Medline

29. A. Kuchina, L. M. Brettner, L. Paleologu, C. M. Roco, A. B. Rosenberg, A. Carignano, R. Kibler, M. Hirano, R. W. DePaolo, G. Seelig, Microbial single-cell RNA sequencing by split-pool barcoding. *Science* **371**, eaba5257 (2021). doi:10.1126/science.aba5257 Medline

30. S. B. Blattman, W. Jiang, P. Oikonomou, S. Tavazoie, Prokaryotic single-cell RNA sequencing by in situ combinatorial indexing. *Nat. Microbiol.* **5**, 1192–1201 (2020). doi:10.1038/s41564-020-0729-6 Medline

31. A. Raj, P. van den Bogaard, S. A. Rifkin, A. van Oudenaarden, S. Tyagi, Imaging individual mRNA molecules using multiple singly labeled probes. *Nat. Methods* **5**, 877–879 (2008). doi:10.1038/nmeth.1253 Medline

32. A. M. Femino, F. S. Fay, K. Fogarty, R. H. Singer, Visualization of single RNA transcripts in situ. *Science* **280**, 585–590 (1998). doi:10.1126/science.280.5363.585 Medline

33. L.-H. So, A. Ghosh, C. Zong, L. A. Sepúlveda, R. Segev, I. Golding, General properties of transcriptional time series in Escherichia coli. *Nat. Genet.* **43**, 554–560 (2011). doi:10.1038/ng.821 Medline

34. H. M. T. Choi, V. A. Beck, N. A. Pierce, Next-generation in situ hybridization chain reaction: Higher gain, lower cost, greater durability. *ACS Nano* **8**, 4284–4294 (2014). doi:10.1021/nn405717p Medline

35. K. H. Chen, A. N. Boettiger, J. R. Moffitt, S. Wang, X. Zhuang, RNA imaging. Spatially resolved, highly multiplexed RNA profiling in single cells. *Science* **348**, aaa6090 (2015). doi:10.1126/science.aaa6090 Medline

36. C. L. Eng, M. Lawson, Q. Zhu, R. Dries, N. Koulena, Y. Takei, J. Yun, C. Cronin, C. Karp, G.-C. Yuan, L. Cai, Transcriptome-scale super-resolved imaging in tissues by RNA seqFISH. *Nature* **568**, 235–239 (2019). doi:10.1038/s41586-019-1049-y Medline

37. E. Lubeck, A. F. Coskun, T. Zhiyentayev, M. Ahmad, L. Cai, Single-cell in situ RNA profiling by sequential hybridization. *Nat. Methods* **11**, 360–361 (2014). doi:10.1038/nmeth.2892 Medline

38. J. R. Moffitt, D. Bambah-Mukku, S. W. Eichhorn, E. Vaughn, K. Shekhar, J. D. Perez, N. D. Rubinstein, J. Hao, A. Regev, C. Dulac, X. Zhuang, Molecular, spatial, and functional single-cell profiling of the hypothalamic preoptic region. *Science* **362**, eaau5324 (2018). doi:10.1126/science.aau5324 Medline

39. S. Shah, E. Lubeck, W. Zhou, L. Cai, In situ transcription profiling of single cells reveals spatial organization of cells in the mouse hippocampus. *Neuron* **92**, 342–357 (2016). doi:10.1016/j.neuron.2016.10.001 Medline

40. A. Lignell, L. Kerosuo, S. J. Streichan, L. Cai, M. E. Bronner, Identification of a neural crest stem cell niche by Spatial Genomic Analysis. *Nat. Commun.* **8**, 1830 (2017). doi:10.1038/s41467-017-01561-w Medline

41. S. Shah, Y. Takei, W. Zhou, E. Lubeck, J. Yun, C. L. Eng, N. Koulena, C. Cronin, C. Karp, E. J. Liaw, M. Amin, L. Cai, Dynamics and spatial genomics of the nascent transcriptome by intron seqFISH. *Cell* **174**, 363–376.e16 (2018). doi:10.1016/j.cell.2018.05.035 Medline

42. S. O. Skinner, L. A. Sepúlveda, H. Xu, I. Golding, Measuring mRNA copy number in individual Escherichia coli cells using single-molecule fluorescent in situ hybridization. *Nat. Protoc.* **8**, 1100–1113 (2013). doi:10.1038/nprot.2013.066 Medline

43. A. Y. Bhagirath, Y. Li, D. Somayajula, M. Dadashi, S. Badr, K. Duan, Cystic fibrosis lung environment and *Pseudomonas aeruginosa* infection. *BMC Pulm. Med.* **16**, 174 (2016). doi:10.1186/s12890-016-0339-5 Medline

44. S. Malhotra, D. Hayes Jr., D. J. Wozniak, Cystic Fibrosis and *Pseudomonas aeruginosa*: The Host-Microbe Interface. *Clin. Microbiol. Rev.* **32**, e00138-18 (2019). doi:10.1128/CMR.00138-18 Medline

45. Y. Takei, J. Yun, S. Zheng, N. Ollikainen, N. Pierson, J. White, S. Shah, J. Thomassie, S. Suo, C. L. Eng, M. Guttman, G.-C. Yuan, L. Cai, Integrated spatial genomics reveals global architecture of single nuclei. *Nature* **590**, 344–350 (2021). doi:10.1038/s41586-020-03126-2 Medline

46. I. Vallet-Gely, F. Boccard, Chromosomal organization and segregation in *Pseudomonas aeruginosa*. *PLOS Genet.* **9**, e1003492 (2013). doi:10.1371/journal.pgen.1003492 Medline

47. J. Lee, L. Zhang, The hierarchy quorum sensing network in *Pseudomonas aeruginosa*. *Protein Cell* **6**, 26–41 (2015). doi:10.1007/s13238-014-0100-x Medline

48. A. Price-Whelan, L. E. P. Dietrich, D. K. Newman, Pyocyanin alters redox homeostasis and carbon flux through central metabolic pathways in *Pseudomonas aeruginosa* PA14. *J. Bacteriol.* **189**, 6372–6381 (2007). doi:10.1128/JB.00505-07 Medline

49. J. Jo, K. L. Cortez, W. C. Cornell, A. Price-Whelan, L. E. Dietrich, An orphan cbb_3-type cytochrome oxidase subunit supports *Pseudomonas aeruginosa* biofilm growth and virulence. *eLife* **6**, e30205 (2017). doi:10.7554/eLife.30205 Medline

50. H. Arai, Regulation and function of versatile aerobic and anaerobic respiratory metabolism in *Pseudomonas aeruginosa*. *Front. Microbiol.* **2**, 103 (2011). doi:10.3389/fmicb.2011.00103 Medline

51. S. Schulz, D. Eckweiler, A. Bielecka, T. Nicolai, R. Franke, A. Dötsch, K. Hornischer, S. Bruchmann, J. Düvel, S. Häussler, Elucidation of sigma factor-associated networks in *Pseudomonas aeruginosa* reveals a modular architecture with limited and function-

specific crosstalk. *PLOS Pathog.* **11**, e1004744 (2015). doi:10.1371/journal.ppat.1004744 Medline

52. S. E. Finkel, Long-term survival during stationary phase: Evolution and the GASP phenotype. *Nat. Rev. Microbiol.* **4**, 113–120 (2006). doi:10.1038/nrmicro1340 Medline

53. L. McInnes, J. Healy, J. Melville, UMAP: Uniform Manifold Approximation and Projection for Dimension Reduction. arXiv:1802.03426 [stat.ML] (9 February 2018).

54. E. Bosdriesz, D. Molenaar, B. Teusink, F. J. Bruggeman, How fast-growing bacteria robustly tune their ribosome concentration to approximate growth-rate maximization. *FEBS J.* **282**, 2029–2044 (2015). doi:10.1111/febs.13258 Medline

55. B. R. Borlee, A. D. Goldman, K. Murakami, R. Samudrala, D. J. Wozniak, M. R. Parsek, *Pseudomonas aeruginosa* uses a cyclic-di-GMP-regulated adhesin to reinforce the biofilm extracellular matrix. *Mol. Microbiol.* **75**, 827–842 (2010). doi:10.1111/j.1365-2958.2009.06991.x Medline

56. C. Reichhardt, C. Wong, D. Passos da Silva, D. J. Wozniak, M. R. Parsek, CdrA: interactions within the *Pseudomonas aeruginosa* biofilm matrix safeguard it from proteolysis and promote cellular packing. *mBio* **9**, e01376 (2018). doi:10.1128/mBio.01376-18 Medline

57. O. Zaborina, C. Holbrook, Y. Chen, J. Long, A. Zaborin, I. Morozova, H. Fernandez, Y. Wang, J. R. Turner, J. C. Alverdy, Structure-function aspects of PstS in multi-drug-resistant *Pseudomonas aeruginosa*. *PLOS Pathog.* **4**, e43 (2008). doi:10.1371/journal.ppat.0040043 Medline

58. M. L. Gil-Marqués, G. Labrador Herrera, A. Miró Canturri, J. Pachón, Y. Smani, M. E. Pachón-Ibáñez, Role of PstS in the pathogenesis of *Acinetobacter baumannii* under microaerobiosis and normoxia. *J. Infect. Dis.* **222**, 1204–1212 (2020). doi:10.1093/infdis/jiaa201 Medline

59. A. R. Hauser, The type III secretion system of *Pseudomonas aeruginosa*: Infection by injection. *Nat. Rev. Microbiol.* **7**, 654–665 (2009). doi:10.1038/nrmicro2199 Medline

60. O. Wurtzel, D. R. Yoder-Himes, K. Han, A. A. Dandekar, S. Edelheit, E. P. Greenberg, R. Sorek, S. Lory, The single-nucleotide resolution transcriptome of *Pseudomonas aeruginosa* grown in body temperature. *PLOS Pathog.* **8**, e1002945 (2012). doi:10.1371/journal.ppat.1002945 Medline

61. C. Lombardi, J. Tolchard, S. Bouillot, L. Signor, C. Gebus, D. Liebl, D. Fenel, J.-M. Teulon, J. Brock, B. Habenstein, J.-L. Pellequer, E. Faudry, A. Loquet, I. Attrée, A. Dessen, V. Job, Structural and functional characterization of the type three secretion system (T3SS) needle of *Pseudomonas aeruginosa*. *Front. Microbiol.* **10**, 573 (2019). doi:10.3389/fmicb.2019.00573 Medline

62. T. Bjarnsholt, P. Ø. Jensen, M. J. Fiandaca, J. Pedersen, C. R. Hansen, C. B. Andersen, T. Pressler, M. Givskov, N. Høiby, *Pseudomonas aeruginosa* biofilms in the respiratory tract of cystic fibrosis patients. *Pediatr. Pulmonol.* **44**, 547–558 (2009). doi:10.1002/ppul.21011 Medline

63. N. Høiby, O. Ciofu, H. K. Johansen, Z. J. Song, C. Moser, P. Ø. Jensen, S. Molin, M. Givskov, T. Tolker-Nielsen, T. Bjarnsholt, The clinical impact of bacterial biofilms. *Int. J. Oral Sci.* **3**, 55–65 (2011). doi:10.4248/IJOS11026 Medline

64. K. L. Palmer, L. M. Aye, M. Whiteley, Nutritional cues control *Pseudomonas aeruginosa* multicellular behavior in cystic fibrosis sputum. *J. Bacteriol.* **189**, 8079–8087 (2007). doi:10.1128/JB.01138-07 Medline

65. G. Gicquel, E. Bouffartigues, M. Bains, V. Oxaran, T. Rosay, O. Lesouhaitier, N. Connil, A. Bazire, O. Maillot, M. Bénard, P. Cornelis, R. E. W. Hancock, A. Dufour, M. G. J. Feuilloley, N. Orange, E. Déziel, S. Chevalier, The extra-cytoplasmic function sigma factor sigX modulates biofilm and virulence-related properties in *Pseudomonas aeruginosa*. *PLOS ONE* **8**, e80407 (2013). doi:10.1371/journal.pone.0080407 Medline

66. L. L. Burrows, *Pseudomonas aeruginosa* twitching motility: Type IV pili in action. *Annu. Rev. Microbiol.* **66**, 493–520 (2012). doi:10.1146/annurev-micro-092611-150055 Medline

67. G. A. O'Toole, R. Kolter, Flagellar and twitching motility are necessary for *Pseudomonas aeruginosa* biofilm development. *Mol. Microbiol.* **30**, 295–304 (1998). doi:10.1046/j.1365-2958.1998.01062.x Medline

68. R. Belas, Biofilms, flagella, and mechanosensing of surfaces by bacteria. *Trends Microbiol.* **22**, 517–527 (2014). doi:10.1016/j.tim.2014.05.002 Medline

69. B.-J. Laventie, M. Sangermani, F. Estermann, P. Manfredi, R. Planes, I. Hug, T. Jaeger, E. Meunier, P. Broz, U. Jenal, A surface-induced asymmetric program promotes tissue colonization by *Pseudomonas aeruginosa*. *Cell Host Microbe* **25**, 140–152.e6 (2019). doi:10.1016/j.chom.2018.11.008 Medline

70. M. G. K. Ghequire, R. De Mot, The tailocin tale: Peeling off phage tails. *Trends Microbiol.* **23**, 587–590 (2015). doi:10.1016/j.tim.2015.07.011 Medline

71. L.-M. Bobay, M. Touchon, E. P. C. Rocha, Pervasive domestication of defective prophages by bacteria. *Proc. Natl. Acad. Sci. U.S.A.* **111**, 12127–12132 (2014). doi:10.1073/pnas.1405336111 Medline

72. L. Turnbull, M. Toyofuku, A. L. Hynen, M. Kurosawa, G. Pessi, N. K. Petty, S. R. Osvath, G. Cárcamo-Oyarce, E. S. Gloag, R. Shimoni, U. Omasits, S. Ito, X. Yap, L. G. Monahan, R. Cavaliere, C. H. Ahrens, I. G. Charles, N. Nomura, L. Eberl, C. B. Whitchurch, Explosive cell lysis as a mechanism for the biogenesis of bacterial membrane vesicles and biofilms. *Nat. Commun.* **7**, 11220 (2016). doi:10.1038/ncomms11220 Medline

73. J. Vacheron, C. M. Heiman, C. Keel, Live cell dynamics of production, explosive release and killing activity of phage tail-like weapons for *Pseudomonas* kin exclusion. *Commun. Biol.* **4**, 87 (2021). doi:10.1038/s42003-020-01581-1 Medline

74. C. B. Whitchurch, T. Tolker-Nielsen, P. C. Ragas, J. S. Mattick, Extracellular DNA required for bacterial biofilm formation. *Science* **295**, 1487 (2002). doi:10.1126/science.295.5559.1487 Medline

75. M. D. Brazas, R. E. W. Hancock, Ciprofloxacin induction of a susceptibility determinant in *Pseudomonas aeruginosa*. *Antimicrob. Agents Chemother.* **49**, 3222–3227 (2005). doi:10.1128/AAC.49.8.3222-3227.2005 Medline

76. T. L. Povolotsky, A. Keren-Paz, I. Kolodkin-Gal, Metabolic microenvironments drive microbial differentiation and antibiotic resistance. *Trends Genet.* **37**, 4–8 (2021). doi:10.1016/j.tig.2020.10.007 Medline

77. A. K. Wessel, T. A. Arshad, M. Fitzpatrick, J. L. Connell, R. T. Bonnecaze, J. B. Shear, M. Whiteley, Oxygen limitation within a bacterial aggregate. *mBio* **5**, e00992 (2014). doi:10.1128/mBio.00992-14 Medline

78. L. E. P. Dietrich, C. Okegbe, A. Price-Whelan, H. Sakhtah, R. C. Hunter, D. K. Newman, Bacterial community morphogenesis is intimately linked to the intracellular redox state. *J. Bacteriol.* **195**, 1371–1380 (2013). doi:10.1128/JB.02273-12 Medline

79. E. S. Cowley, S. H. Kopf, A. LaRiviere, W. Ziebis, D. K. Newman, Pediatric cystic fibrosis sputum can be chemically dynamic, anoxic, and extremely reduced due to hydrogen sulfide formation. *mBio* **6**, e00767 (2015). doi:10.1128/mBio.00767-15 Medline

80. S. S. Yoon, R. F. Hennigan, G. M. Hilliard, U. A. Ochsner, K. Parvatiyar, M. C. Kamani, H. L. Allen, T. R. DeKievit, P. R. Gardner, U. Schwab, J. J. Rowe, B. H. Iglewski, T. R. McDermott, R. P. Mason, D. J. Wozniak, R. E. W. Hancock, M. R. Parsek, T. L. Noah, R. C. Boucher, D. J. Hassett, *Pseudomonas aeruginosa* anaerobic respiration in biofilms: Relationships to cystic fibrosis pathogenesis. *Dev. Cell* **3**, 593–603 (2002). doi:10.1016/S1534-5807(02)00295-2 Medline

81. M. Eschbach, K. Schreiber, K. Trunk, J. Buer, D. Jahn, M. Schobert, Long-term anaerobic survival of the opportunistic pathogen *Pseudomonas aeruginosa* via pyruvate fermentation. *J. Bacteriol.* **186**, 4596–4604 (2004). doi:10.1128/JB.186.14.4596-4604.2004 Medline

82. D. J. Hassett, L. Charniga, K. Bean, D. E. Ohman, M. S. Cohen, Response of *Pseudomonas aeruginosa* to pyocyanin: Mechanisms of resistance, antioxidant defenses, and demonstration of a manganese-cofactored superoxide dismutase. *Infect. Immun.* **60**, 328–336 (1992). doi:10.1128/iai.60.2.328-336.1992 Medline

83. S. M. Brown, M. L. Howell, M. L. Vasil, A. J. Anderson, D. J. Hassett, Cloning and characterization of the katB gene of *Pseudomonas aeruginosa* encoding a hydrogen peroxide-inducible catalase: Purification of KatB, cellular localization, and demonstration that it is essential for optimal resistance to hydrogen peroxide. *J. Bacteriol.* **177**, 6536–6544 (1995). doi:10.1128/jb.177.22.6536-6544.1995 Medline

84. S. Su, W. Panmanee, J. J. Wilson, H. K. Mahtani, Q. Li, B. D. Vanderwielen, T. M. Makris, M. Rogers, C. McDaniel, J. D. Lipscomb, R. T. Irvin, M. J. Schurr, J. R. Lancaster Jr., R. A. Kovall, D. J. Hassett, Catalase (KatA) plays a role in protection against anaerobic nitric oxide in *Pseudomonas aeruginosa*. *PLOS ONE* **9**, e91813 (2014). doi:10.1371/journal.pone.0091813 Medline

85. F. Cutruzzolà, N. Frankenberg-Dinkel, Origin and impact of nitric oxide in *Pseudomonas aeruginosa* biofilms. *J. Bacteriol.* **198**, 55–65 (2016). doi:10.1128/JB.00371-15 Medline

86. D. W. Basta, M. Bergkessel, D. K. Newman, Identification of fitness determinants during energy-limited growth arrest in *Pseudomonas aeruginosa*. *mBio* **8**, e01170 (2017). doi:10.1128/mBio.01170-17 Medline

87. U. A. Ochsner, M. L. Vasil, E. Alsabbagh, K. Parvatiyar, D. J. Hassett, Role of the *Pseudomonas aeruginosa* oxyR-recG operon in oxidative stress defense and DNA repair: OxyR-dependent regulation of katB-ankB, ahpB, and ahpC-ahpF. *J. Bacteriol.* **182**, 4533–4544 (2000). doi:10.1128/JB.182.16.4533-4544.2000 Medline

88. M. Toyofuku, N. Nomura, T. Fujii, N. Takaya, H. Maseda, I. Sawada, T. Nakajima, H. Uchiyama, Quorum sensing regulates denitrification in *Pseudomonas aeruginosa* PAO1. *J. Bacteriol.* **189**, 4969–4972 (2007). doi:10.1128/JB.00289-07 Medline

89. N. E. Van Alst, L. A. Sherrill, B. H. Iglewski, C. G. Haidaris, Compensatory periplasmic nitrate reductase activity supports anaerobic growth of *Pseudomonas aeruginosa* PAO1 in the absence of membrane nitrate reductase. *Can. J. Microbiol.* **55**, 1133–1144 (2009). doi:10.1139/W09-065 Medline

90. K. Schreiber, N. Boes, M. Eschbach, L. Jaensch, J. Wehland, T. Bjarnsholt, M. Givskov, M. Hentzer, M. Schobert, Anaerobic survival of *Pseudomonas aeruginosa* by pyruvate fermentation requires an Usp-type stress protein. *J. Bacteriol.* **188**, 659–668 (2006). doi:10.1128/JB.188.2.659-668.2006 Medline

91. S. K. Dolan, M. Welch, The glyoxylate shunt, 60 years on. *Annu. Rev. Microbiol.* **72**, 309–330 (2018). doi:10.1146/annurev-micro-090817-062257 Medline

92. A. Crousilles, S. K. Dolan, P. Brear, D. Y. Chirgadze, M. Welch, Gluconeogenic precursor availability regulates flux through the glyoxylate shunt in *Pseudomonas aeruginosa*. *J. Biol. Chem.* **293**, 14260–14269 (2018). doi:10.1074/jbc.RA118.004514 Medline

93. S. K. Dolan, G. Pereira, R. Silva-Rocha, M. Welch, Transcriptional regulation of central carbon metabolism in *Pseudomonas aeruginosa*. *Microb. Biotechnol.* **13**, 285–289 (2020). doi:10.1111/1751-7915.13423 Medline

94. T. Kawakami, M. Kuroki, M. Ishii, Y. Igarashi, H. Arai, Differential expression of multiple terminal oxidases for aerobic respiration in *Pseudomonas aeruginosa*. *Environ. Microbiol.* **12**, 1399–1412 (2010). Medline

95. A. M. Stern, J. Zhu, An introduction to nitric oxide sensing and response in bacteria. *Adv. Appl. Microbiol.* **87**, 187–220 (2014). doi:10.1016/B978-0-12-800261-2.00005-0 Medline

96. A. Edelstein, N. Amodaj, K. Hoover, R. Vale, N. Stuurman, Computer control of microscopes using μManager. *Curr. Protoc. Mol. Biol.* **Chapter 14**, 20 (2010). Medline

97. C. A. Schneider, W. S. Rasband, K. W. Eliceiri, NIH Image to ImageJ: 25 years of image analysis. *Nat. Methods* **9**, 671–675 (2012). doi:10.1038/nmeth.2089 Medline

98. S. Stylianidou, C. Brennan, S. B. Nissen, N. J. Kuwada, P. A. Wiggins, SuperSegger: Robust image segmentation, analysis and lineage tracking of bacterial cells. *Mol. Microbiol.* **102**, 690–700 (2016). doi:10.1111/mmi.13486 Medline

99. F. A. Wolf, P. Angerer, F. J. Theis, SCANPY: Large-scale single-cell gene expression data analysis. *Genome Biol.* **19**, 15 (2018). doi:10.1186/s13059-017-1382-0 Medline

100. R. Milo, P. Jorgensen, U. Moran, G. Weber, M. Springer, BioNumbers—The database of key numbers in molecular and cell biology. *Nucleic Acids Res.* **38** (suppl_1), D750–D753 (2010). doi:10.1093/nar/gkp889 Medline

101. S. Berg, D. Kutra, T. Kroeger, C. N. Straehle, B. X. Kausler, C. Haubold, M. Schiegg, J. Ales, T. Beier, M. Rudy, K. Eren, J. I. Cervantes, B. Xu, F. Beuttenmueller, A. Wolny, C. Zhang, U. Koethe, F. A. Hamprecht, A. Kreshuk, ilastik: Interactive machine learning for (bio)image analysis. *Nat. Methods* **16**, 1226–1232 (2019). doi:10.1038/s41592-019-0582-9 Medline

102. B. Langmead, S. L. Salzberg, Fast gapped-read alignment with Bowtie 2. *Nat. Methods* **9**, 357–359 (2012). doi:10.1038/nmeth.1923 Medline

103. Y. Liao, G. K. Smyth, W. Shi, featureCounts: An efficient general purpose program for assigning sequence reads to genomic features. *Bioinformatics* **30**, 923–930 (2014). doi:10.1093/bioinformatics/btt656 Medline

104. Y. Zhang, Z. Hu, Combined treatment of *Pseudomonas aeruginosa* biofilms with bacteriophages and chlorine. *Biotechnol. Bioeng.* **110**, 286–295 (2013). doi:10.1002/bit.24630 Medline

105. D. Dar, N. Dar, L. Cai, D. K. Newman, Data for: Spatial transcriptomics of planktonic and sessile bacterial populations at single-cell resolution, Zenodo (2021); http://doi.org/10.5281/zenodo.4767568.

106. D. Dar, N. Dar, L. Cai, D. K. Newman, Imaging data for: Spatial transcriptomics of planktonic and sessile bacterial populations at single-cell resolution, Zenodo (2021); http://doi.org/10.5281/zenodo.4771778.